TUM School of Engineering and Design
Technical University of Munich

Three-component measurement of an aircraft with and without horizontal stabilizer

Experiment 7

Final Report for Practical Course: Aerodynamic of Aircraft
at the TUM School of Engineering and Design of the Technical University of Munich

Submitted by Gabriel Virto Chirhuana

Supervised by Stefan Hayböck, M.Sc.
Chair of Aerodynamics and Fluid Mechanics

Period December 10, 2025 until December 17, 2025

0.1 Introduction

The present report corresponds to Experiment 7, entitled *"Three-Component Measurement on an Aircraft"*, which is part of the practical course *Aerodynamics of Aircraft*.

In this experimental test, the forces and pitching moment acting on an aircraft model are investigated using a three-component balance in a wind tunnel, focusing on static longitudinal stability. The experimental setup and measurement procedure are described in detail in the chapter *Experimental Setup*. Four measurement configurations are examined: aircraft configurations with and without a horizontal stabilizer, each tested at two flap deflection angles of 0° and 60°. For all configurations, the angle of attack is varied in the range from −6° to +6°.

The final chapter presents and discusses the experimental results with the objective of assessing the static stability characteristics of the aircraft. The lift, drag, and pitching moment coefficients are evaluated as functions of the angle of attack. Particular emphasis is placed on the influence of the horizontal stabilizer, the determination of the neutral point position and the experimental verification of theoretical stability criteria.

0.2 Theoretical Background

0.2.1 Static Longitudinal Stability

Longitudinal static stability refers how the aircraft reacts to small disturbances in the angle of attack. An aircraft is statically stable if a small increase in angle of attack generates a restoring pitching moment that tends to reduce the disturbance and return the aircraft to its original equilibrium condition [2].

0.2.2 Stability Criterion

The criterion for longitudinal static stability is given by

$$\frac{\partial C_M}{\partial \alpha} < 0. \tag{1}$$

A negative slope of the pitching moment coefficient with respect to the angle of attack indicates that an increase in α produces a nose-down pitching moment, which stabilizes the aircraft. Conversely, a positive slope corresponds to an unstable configuration, as no restoring moment is generated. [1]

The Fig.1 shows how a disturbance in angle of attack leads to a restoring or destabilizing pitching moment depending on the slope of the C_M curve. In the present experiment, this criterion is evaluated by comparing the measured pitching moment behavior for configurations with and without a horizontal stabilizer.

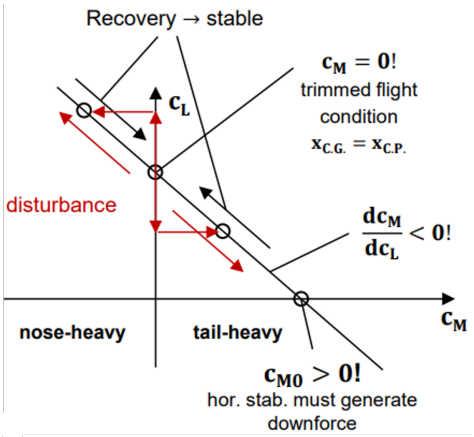

Figure 1: Stability criterion [2]

0.2.3 Neutral Point and Static Margin

The neutral point is defined as the position of the center of gravity at which the aircraft becomes neutrally stable [1]. The position of the neutral point can be expressed in non-dimensional form as

$$\frac{x_N}{l_\mu} = \frac{\partial C_M}{\partial C_L}, \tag{2}$$

where x_N indicates the location of the neutral point and l_μ represents the mean aerodynamic chord.

An aircraft is considered statically stable when its center of gravity is located in front of the neutral point. The distance between the center of gravity and the neutral point quantifies the aircraft's longitudinal stability.

0.2.4 Role of the Horizontal Stabilizer

The horizontal stabilizer plays a key role in providing longitudinal static stability. Rather than generating lift, it is mainly designed to create a stabilizing pitching moment. Because it is set at a negative incidence angle relative to the wing chord, the stabilizer produces a downward force at small angles of attack, resulting in a nose-down pitching moment that helps restore equilibrium.

Having a horizontal stabilizer shifts the neutral point further back and ensures that the pitching moment coefficient decreases with increasing angle of attack. In comparison, aircraft without a horizontal stabilizer usually have the opposite behavior, making them longitudinally unstable. In this experiment, the stabilizing effect of the horizontal stabilizer is assessed by comparing the pitching moment behavior and neutral point position for configurations with and without the stabilizer.

0.3 Experimental setup

0.3.1 SIAT 223

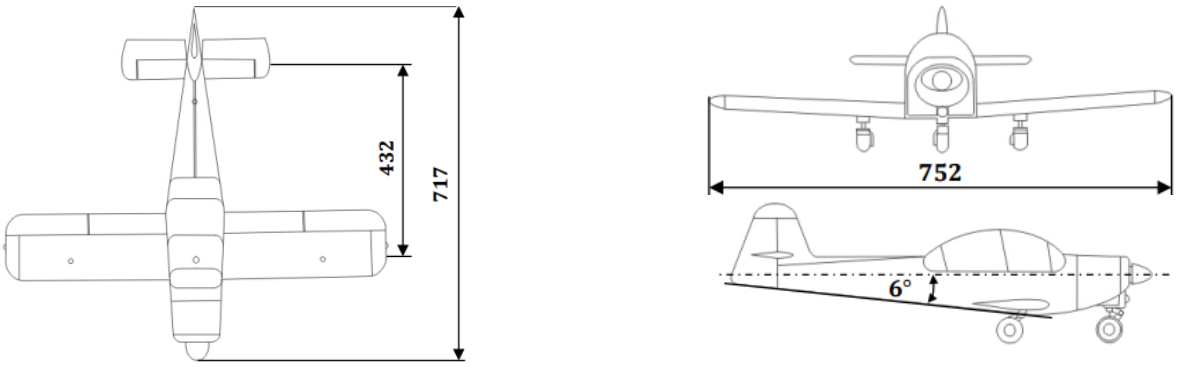

Figure 2: Wind tunnel model of the SIAT 223 aircraft type [1]

This experiment uses a model based on a SIAT aircraft, scaled down to 1:10. The most important technical specifications of the SIAT original aircraft include an engine power in the range of 160 to 200 PS and a take-off weight between 700 and 1000 kg. The aircraft has a cruise speed of approximately 230 km/h and a landing speed between 80 and 90 km/h. The maximum operational range is about 1450 km.

In addition to these characteristics, the geometry of the wing and horizontal stabilizer relevant for the aerodynamic analysis. The model's wing has a area of $A_{\text{wing}} = 0.105\,\text{m}^2$ and an aspect ratio of $\Lambda = 5.37$. The horizontal stabilizer has values of $A_{\text{stabilizer}} = 0.025\,\text{m}^2$ and $\Lambda = 3.98$. Other geometric dimensions of the aircraft model are illustrated in Fig.2. The incidence angle of the horizontal tailplane relative to the wing chord is set to $\varepsilon_{\text{HT}} = -3°$.

0.3.2 Procedure and Data Processing

A total of 28 individual measurements are conducted during the experiment. All measurements are conducted for configurations with and without a horizontal stabilizer. The measurements are performed for two extra configurations: retracted flaps ($\eta_L = 0°$) and fully extended flaps ($\eta_L = 60°$). For each flap configuration, the angle of attack is varied over the range $\alpha = -6°, -4°, -2°, 0°, 2°, 4°$ and $6°$.

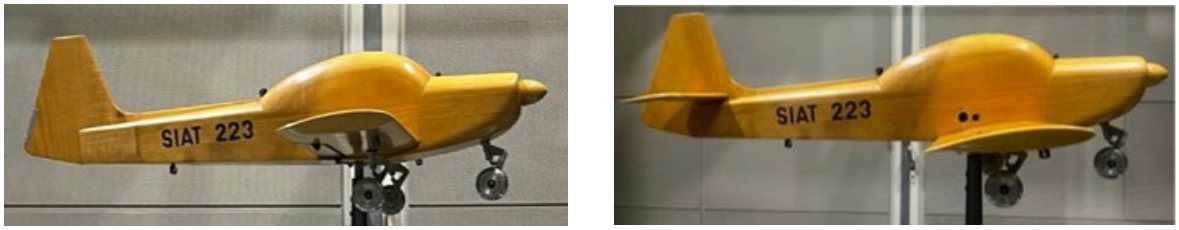

Without the horizontal stabilizer

With the horizontal stabilizer

Figure 3: Two configurations of the aircraft model

During each measurement, the three-component balance measured the raw force components Z' and X', corresponding to lift and drag, as well as the raw pitching moment M'_y. Prior to the measurements, the balance system is dynamically calibrated in order to account for systematic effects of the measurement setup. The calibration offsets are given by

$$Z_0 = 1.1\ \text{N}, \qquad X_0 = 11.5\ \text{N}, \qquad M_{y0} = 6.3\ \text{N m}. \tag{3}$$

Using these offsets, the corrected forces and pitching moment are obtained as

$$Z = Z' - Z_0, \quad X = X' - X_0, \quad M_y = M'_y - M_{y0} - X \cdot z_B - Z \cdot x_B, \tag{4}$$

where x_B and z_B denote the geometric distances between the balance reference point and the aircraft reference point.

The aerodynamic reference conditions are defined by the ambient conditions in the wind tunnel. During the experiment, the ambient pressure and temperature are $p_\infty = 963\,\text{mbar}$ and $T_0 = 21°\text{C}$, respectively. This corresponds to an air density of $\rho_\infty = 1.14\,\text{kg m}^{-3}$ and a kinematic viscosity of $\nu = 1.60 \times 10^{-5}\,\text{m}^2\,\text{s}^{-1}$. The dynamic pressure is measured as $q_\infty = 9\,\text{mbar}$ and is defined by

$$q_\infty = \frac{1}{2}\rho_\infty V_\infty^2. \tag{5}$$

From this relation, the free-stream velocity in the wind tunnel is obtained as

$$V_\infty = \sqrt{\frac{2q_\infty}{\rho_\infty}} = 39.7\,\text{m s}^{-1}. \tag{6}$$

In a subsequent step, the corrected forces and pitching moment are converted into non-dimensional aerodynamic coefficients using the dynamic pressure q_∞, the wing reference area S, and the mean aerodynamic chord l_μ:

$$C_L = \frac{Z}{q_\infty S}, \quad C_D = \frac{X}{q_\infty S}, \quad C_M = \frac{M_y}{q_\infty S l_\mu}. \tag{7}$$

These coefficients standardize the aircraft's aerodynamic behavior, making it easier to compare results from different test setups. Using these values, the relationships between lift,

drag, and pitching moment as functions of angle of attack are analyzed. Additionally, the drag polar $C_L(C_D)$ and the lift–moment curve $C_L(C_M)$ are examined to evaluate aerodynamic efficiency and the longitudinal stability behavior.

The position of the neutral point is determined from the slope of the lift–moment relationship according to

$$\frac{x_N}{l_\mu} = \frac{\partial C_M}{\partial C_L}, \tag{8}$$

which represents the longitudinal location at which the aircraft becomes neutrally stable. Furthermore, the center-of-pressure position is approximated by

$$\frac{x_P}{l_\mu} \approx \frac{C_M}{C_L}, \tag{9}$$

assuming small angles of attack.

The resulting aerodynamic and stability parameters are summarized in Table 1. The table shows the influence of flap deflection and the horizontal stabilizer on the lift and pitching moment characteristics. Notably, changes in the pitching moment slope and the neutral point's position demonstrate the stabilizing role of the horizontal stabilizer, while flap deflection mainly shifts the lift and the zero-lift angle.

		without HS		**with HS**	
Quantity	**Symbol**	$\eta_L = 0°$	$\eta_L = 60°$	$\eta_L = 0°$	$\eta_L = 60°$
Lift curve slope	$C_{L\alpha}$ [$^{\circ -1}$]	3.581	3.657	4.175	4.175
Zero-lift angle of attack	α_0 [°]	-3.64	-10.03	-2.95	-8.01
Pitching moment slope	$C_{M\alpha}$ [$^{\circ -1}$]	0.523	0.535	-1.055	-0.928
Zero-lift moment coefficient	C_{M0} [-]	-0.031	-0.178	0.120	0.211
Neutral point position	x_N/l_μ [-]	-0.146	-0.146	0.253	0.222

Table 1: Coefficients as a function of flap deflection η_L, with and without the horizontal stabilizer

0.4 Results

0.4.1 Lift coefficient as a function of angle of attack

The lift coefficient as a function of the angle of attack, shown in Fig. 4, indicates that all measurements were conducted within the linear lift regime. At negative angles of attack, the lift coefficient is small or negative, while it increases continuously with increasing angle of attack for all configurations.

The flap deflection has a relevant influence on the lift behavior. With flaps deflected to 60°, the lift coefficient is increased over the entire angle-of-attack range and the zero-lift angle of attack shifts towards more negative values. This shift results from the increased camber of the wing.

The influence of the horizontal stabilizer is most evident at small angles of attack. Due to its negative incidence angle of $\varepsilon_{HT} = -3°$, the stabilizer generates a downforce, which reduces the total lift of the aircraft in this regime. As the angle of attack increases, the stabilizer contributes to the lift. Consequently, the differences between configurations with and without the horizontal stabilizer decrease at higher angles of attack.

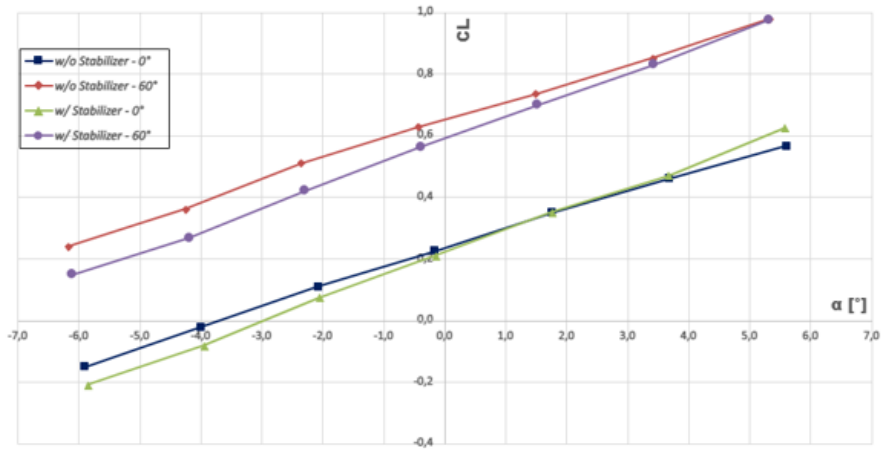

Figure 4: Lift coefficient as a function of AoA

0.4.2 Drag coefficient as a function of angle of attack

Flap deflection has a pronounced influence on the drag behavior, as shown in Fig. 5. With flaps deflected, the drag coefficient increases significantly, approximately twice as high. This increase can be attributed to the higher wing camber, which enhances flow separation.

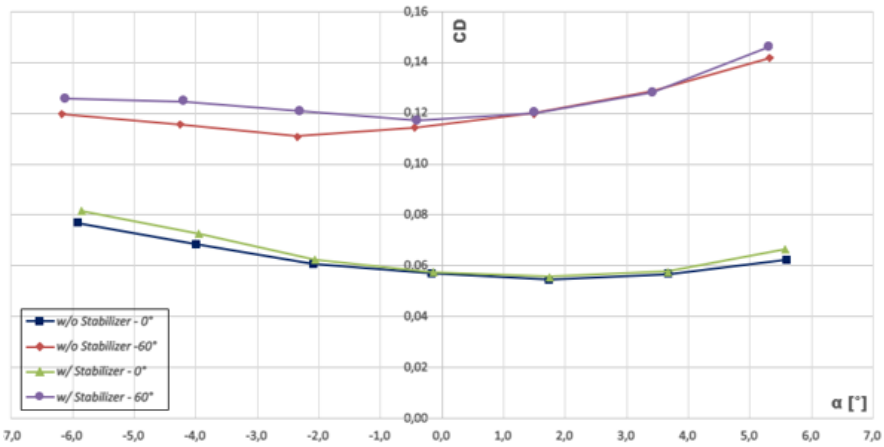

Figure 5: Drag coefficient as a function of AoA

Additionally, the configuration with the horizontal stabilizer exhibits slightly higher drag values than the configuration without one. This additional drag originates from the surface area of the stabilizer itself and from increased induced drag due to the stabilizer downforce required for longitudinal trim. Although this leads to a drag penalty, the horizontal stabilizer plays a crucial role in ensuring longitudinal static stability.

0.4.3 Pitching moment coefficient as a function of the angle of attack

The following Fig.6 provides a direct insight into the longitudinal static stability of the aircraft. The slope of the $C_M(\alpha)$ curve represents the stability criterion: a negative slope indicates a statically stable configuration, whereas a positive slope corresponds to instability.

For the configurations without the horizontal stabilizer, the pitching moment coefficient increases with increasing AoA for both flap settings. In the case of $\eta_L = 0°$, the moment

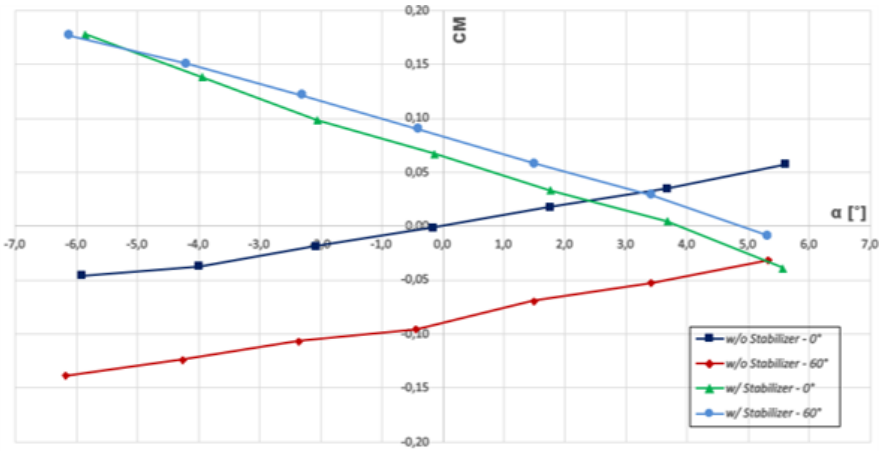

Figure 6: Moment coefficient as a function of AoA

coefficient changes from negative to positive values, while for $\eta_L = 60°$ it remains negative but still exhibits a positive slope. In both cases, the positive slope indicates instability. Flap deflection shifts the pitching moment to more negative values but does not alter the stability behavior.

When the horizontal stabilizer is mounted, a clear stabilizing effect is observed. For both flap deflections, the pitching moment coefficient decreases with increasing angle of attack, resulting in a negative slope and thus static stability. At low angles of attack, the stabilizer contribution dominates the pitching moment, which explains the intersection of the curves for different flap deflections. With increasing AoA, the influence of the wing and flaps becomes more pronounced and the curves separate again. In conclusion, the horizontal stabilizer affects the stability behavior, while flap deflection primarily affects the moment level.

0.4.4 Lift-Drag polar

The Fig.7 shows the aerodynamic efficiency. All configurations exhibit a curved, parabolic shape, which is characteristic of aircraft drag polars. As the lift coefficient increases, the drag coefficient initially rises moderately and then increases more rapidly at higher lift values. This behavior is typical, as induced drag becomes increasingly dominant at higher lift coefficients.

Flap deflection has a pronounced impact on the drag polar. For a flap deflection, the drag coefficient is significantly higher for a given lift compared to the clean configuration. This shift indicates a reduction in aerodynamic efficiency and can be attributed primarily to the increased wing camber, enhanced flow separation, and higher pressure drag associated with large flap deflections.

The presence of the horizontal stabilizer leads to a slight increase in drag at a given lift coefficient. This additional drag arises from the stabilizer surface itself and from increased induced drag resulting from the stabilizer's downforce required for trim. Although this results in a modest drag penalty, it represents a necessary trade-off to ensure static stability.

0.4.5 Lift and pitching moment relationship

The lift-pitching moment relationship shown in Fig. 8 illustrates that the slope of this relationship is directly related to the position of the neutral point and therefore provides key information about the longitudinal static stability of the aircraft.

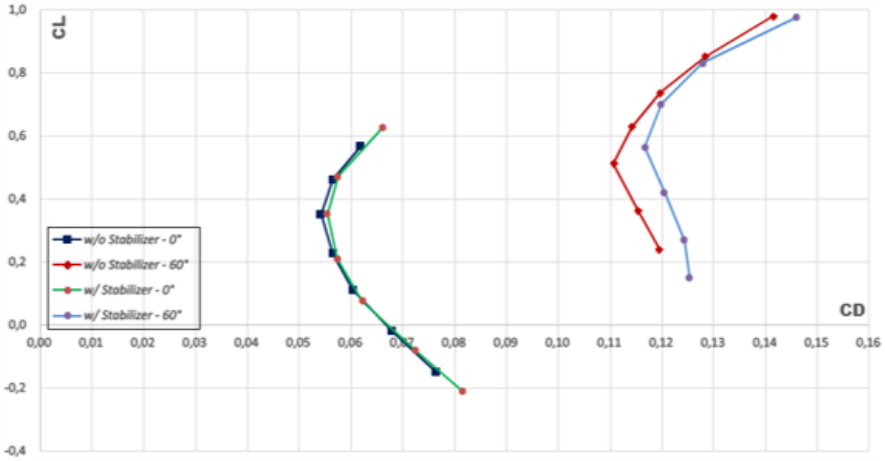

Figure 7: Lift–Drag Polar

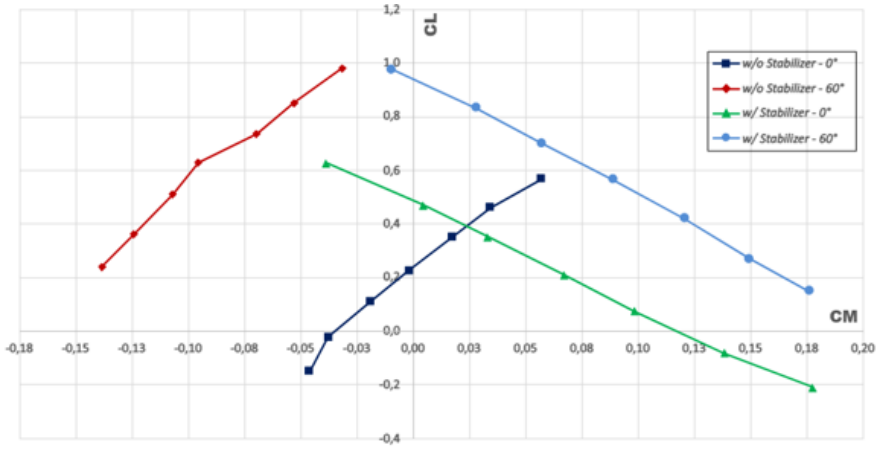

Figure 8: Lift-Pitching Moment Relationship

All configurations exhibit an approximately linear relationship between C_L and C_M. For the configurations without the horizontal stabilizer, an increase in lift is accompanied by an increase in pitching moment, resulting in a positive slope $\partial C_M / \partial C_L > 0$. This behavior implies that the aircraft generates a nose-up pitching moment as lift increases resulting in instability.

Flap deflection shifts the $C_L(C_M)$ curves to higher lift values due to the increased wing camber, while the slope of the curves remains unchanged. This demonstrates that flap deflection primarily affects the lift level but does not improve stability independently.

In contrast, the configurations with the horizontal stabilizer exhibit a negative slope. In this case, increasing lift leads to a decrease in pitching moment, corresponding to $\partial C_M / \partial C_L < 0$, which indicates longitudinal static stability. For both flap deflections, the stabilizing effect of the horizontal stabilizer is preserved, confirming that the stabilizer is the dominant component governing the aircraft's longitudinal static stability.

0.5 Conclusions

This experiment investigated the aerodynamic forces and pitching moments acting on an aircraft model using a three-component balance in a wind tunnel. Measurements were carried

out for configurations with and without a horizontal stabilizer and for flap deflections of 0° and 60°, covering an angle-of-attack range from −6° to +6°. The main goal was to find the lift, drag, and pitching moment coefficients and to assess the aircraft's longitudinal static stability.

The lift measurements showed a linear relationship between the lift coefficient and the angle of attack for all configurations. Flap deflection at 60° resulted in a pronounced increase in lift. The presence of the horizontal stabilizer led to a reduction in total lift at small angles of attack due to stabilizer-induced downforce and this influence decreased at higher angles of attack.

A significant increase in drag was observed for the configuration with extended flaps, resulting from increased camber and flow separation. The configuration with the horizontal stabilizer exhibited slightly higher drag levels, which can be attributed to the surface area of the stabilizer and the induced drag associated with downforce.

The pitching moment measurements clearly demonstrated the stabilizing effect of the horizontal stabilizer. Without the stabilizer, the pitching moment coefficient increased with angle of attack, indicating a positive pitching-moment slope and an unstable configuration. With the stabilizer installed, the pitching moment coefficient decreased with angle of attack, resulting in a negative slope and longitudinal static stability. Flap deflection mainly shifted the pitching moment level but did not significantly affect the stability behavior.

This behavior was confirmed by the lift–pitching moment relationship and the calculated neutral point positions. Without the horizontal stabilizer, the neutral point was located forward of the reference point; however, the stabilizer shifted the neutral point rearward. This rearward shift explains the stabilizing effect observed in the pitching moment measurements.

Overall, the experimental results show good agreement with aerodynamic theory. Flap deflection significantly influences lift and drag characteristics, while the horizontal stabilizer is a key element in achieving longitudinal static stability.

The wind tunnel measurements provide experimental verification of the theoretical longitudinal stability criterion.

Appendix 1

η_L [°]	a [°]	Values read			Correction from calibration		
		Z' [N]	X' [N]	M'_y [N m]	Z [N]	X [N]	M_y [N m]
0	-6	-13.28	18.78	11.32	-14.38	7.28	-0.61
0	-4	-1.08	17.96	11.38	-2.18	6.46	-0.50
0	-2	11.37	17.24	11.68	10.27	5.74	-0.25
0	0	22.33	16.93	12.23	21.23	5.43	-0.03
0	2	34.11	16.78	13.01	33.01	5.28	0.23
0	4	44.55	17.11	14.09	43.45	5.61	0.45
0	6	54.70	17.74	15.52	53.60	6.24	0.76
60	-6	23.72	22.89	15.76	22.62	11.39	-1.84
60	-4	35.20	22.59	16.32	34.10	11.09	-1.65
60	-2	49.39	22.29	17.06	48.30	10.79	-1.42
60	0	60.53	22.78	18.26	59.40	11.28	-1.27
60	2	70.72	23.46	19.76	69.60	11.96	-0.93
60	4	81.70	24.50	21.51	80.60	13.00	-0.70
60	6	93.76	26.01	23.79	92.66	14.51	-0.42
0	-6	-18.88	19.28	14.42	-19.98	7.78	2.35
0	-4	-6.74	18.38	13.78	-7.80	6.88	1.83
0	-2	8.05	17.41	13.20	7.00	5.91	1.30
0	0	20.85	16.99	13.12	19.80	5.49	0.89
0	2	34.26	16.90	13.33	33.20	5.40	0.44
0	4	45.52	17.20	13.83	44.40	5.70	0.06
0	6	60.28	18.22	14.97	59.18	6.72	-0.52
60	-6	15.01	23.41	19.92	13.91	11.91	2.34
60	-4	26.36	23.36	20.15	25.30	11.86	1.99
60	-2	40.73	23.12	20.34	39.60	11.62	1.60
60	0	54.35	22.93	20.50	53.20	11.43	1.18
60	2	67.26	23.41	21.22	66.20	11.91	0.76
60	4	79.65	24.41	22.39	78.50	12.91	0.37
60	6	93.37	26.41	24.42	92.27	14.91	-0.12

Table 2: Measured and corrected forces and pitching moments for all configurations

η_L [°]	α_{corr} [°]	C_L [-]	$C_{D,\text{corr}}$ [-]	C_M [-]	x_N/l_μ [-]	x_P/l_μ [-]
0	-5.90	-0.152	0.077	-0.05	-0.065	-0.304
0	-3.98	-0.023	0.068	-0.04	-0.104	-1.642
0	-2.07	0.108	0.060	-0.02	-0.145	0.176
0	-0.15	0.224	0.057	0.00	-0.151	0.009
0	1.76	0.348	0.054	0.02	-0.154	-0.050
0	3.68	0.459	0.057	0.03	-0.183	-0.075
0	5.61	0.566	0.062	0.06	-0.214	-0.101
60	-6.16	0.239	0.120	-0.14	-0.120	0.581
60	-4.25	0.360	0.115	-0.12	-0.117	0.345
60	-2.35	0.510	0.111	-0.11	-0.106	0.210
60	-0.43	0.627	0.114	-0.10	-0.168	0.153
60	1.50	0.735	0.120	-0.07	-0.193	0.095
60	3.42	0.851	0.129	-0.05	-0.156	0.062
60	5.33	0.978	0.142	-0.03	-0.165	0.033
0	-5.86	-0.211	0.082	0.18	0.307	0.842
0	-3.94	-0.083	0.073	0.14	0.282	1.670
0	-2.05	0.073	0.062	0.10	0.244	-1.336
0	-0.14	0.208	0.057	0.07	0.235	-0.320
0	1.76	0.350	0.056	0.03	0.240	-0.094
0	3.68	0.469	0.058	0.00	0.260	-0.009
0	5.57	0.625	0.066	-0.04	0.278	0.062
60	-6.10	0.147	0.125	0.18	0.222	-1.202
60	-4.18	0.267	0.124	0.15	0.206	-0.562
60	-2.29	0.418	0.121	0.12	0.206	-0.289
60	-0.39	0.562	0.117	0.09	0.228	-0.159
60	1.52	0.698	0.120	0.06	0.228	-0.082
60	3.43	0.829	0.128	0.03	0.240	-0.034

Table 3: Aerodynamic coefficients and derived stability quantities for all configurations

Bibliography

[1] Breitsamter, C. *Practical Course: Aerodynamics of the Aircraft*. Course script. 2025.

[2] Hayböck, S. *3-Component Measurement on an Aircraft With and Without Horizontal Stabilizer*. Lecture slides. 2025.